ELSEVIER

Materials Science and Engineering A354 (2003) 217–228

MATERIALS SCIENCE & ENGINEERING A

www.elsevier.com/locate/msea

Recrystallization behavior of a cold-rolled niobium bicrystal

H.R.Z. Sandim [a,*], J.F.C. Lins [a], A.L. Pinto [b], A.F. Padilha [c]

[a] *Departamento de Engenharia de Materiais, DEMAR/FAENQUIL, PO Box 116, Lorena, SP 12600-000, Brazil*
[b] *Instituto Militar de Engenharia, IME, Rio de Janeiro, RJ, 22290-270, Brazil*
[c] *Departamento de Engenharia Metalúrgica e de Materiais, Escola Politécnica, USP, São Paulo, SP, 05508-900, Brazil*

Received 19 February 2002

Abstract

A high-purity coarse-grained niobium bicrystal was 70% cold rolled in multiple passes. Deformation occurred in an inhomogeneous manner in both grains giving rise to a banded structure. In consequence, highly misoriented boundaries were developed in the microstructure in a wide range of misorientations, many reaching about 55°. These boundaries act as effective nucleation sites for recrystallization. The microstructure of both grains was investigated using electron backscatter diffraction (EBSD) in the cold-worked state in order to quantify the misorientations (ψ) associated to these bands. Upon annealing at 800 and 900 °C, the new recrystallized grains were nucleated preferentially at deformation heterogeneities and in the vicinity of the prior grain boundary in this bicrystal.

Keywords: Niobium; Bicrystal; Deformation bands; Misorientation; Recrystallization; EBSD

1. Introduction

The behavior upon deformation of niobium ingots obtained by electron-beam melting differs significantly from bars or plates processed by powder metallurgy (P/M). High-purity niobium ingots processed by such technique are composed of a few very-coarse columnar grains with sizes in the centimeter range. A significant portion of the grains subdivides inhomogeneously favoring the occurrence of deformation heterogeneities. When deformation banding (DB) occurs, different parts of the same grain rotate to distinct end orientations with increasing strain by action of different combinations of slip systems [1]. These distinct volumes are bounded by highly-misoriented boundaries consisting of two-dimensional arrays of geometrically necessary dislocations. Since these bands are usually visible at naked eye, they have also been named macro-scale bands to differentiate them from other structures like microbands, for instance, which can be resolved only by transmission electron microscopy (TEM).

In contrast, P/M products have a finer microstructure consisting of equiaxed grains with sizes below 100 μm, in average. The final grain size depends mostly on the initial powder particle size and the sintering temperature. Deformation heterogeneities, in special deformation bands, are rarely observed (or eventually supressed) in P/M niobium products during plastic deformation due to their smaller grain size. In consequence, the beginning of recrystallization is governed by local inhomogeneities provided by the larger grain boundary area available in the microstructure.

The use of automated electron backscatter diffraction (EBSD) to map large areas in refractory metals and their alloys was already foretold a few years ago [2]. The EBSD technique has been indicated for investigating plastic deformation and subsequent recovery and recrystallization in many metallic materials [3,4]. The nature and morphology of dislocation structures developed during deformation cannot be resolved by this technique, however, EBSD has many advantages including the possibility of obtaining detailed orientation maps faster than in TEM investigation; in addition, bulk

* Corresponding author. Tel.: +55-12-3159-9916; fax: +55-12-553-3006.
E-mail address: hsandim@demar.faenquil.br (H.R.Z. Sandim).

0921-5093/03/$ - see front matter
doi:10.1016/S0921-5093(03)00011-X

specimens can be investigated avoiding thinning to electron transparency as required in TEM.

In the present paper, grain subdivision has formed a macro-scale banded structure in two adjacent grains during cold rolling. Banding was inhomogeneous even within individual grains. The misorientation across boundaries introduced by the development of deformation bands during cold rolling in a coarse niobium bicrystal was determined using EBSD in the scanning electron microscope (SEM). Microstructural aspects like band morphology and band spacing were also investigated in both grains. Upon annealing, recrystallization was found to start predominantly at these deformation heterogeneities and at grain boundary region, in a lesser extent. The misorientations (ψ) observed across the bands reached up to 55° in both grains.

2. Experimental procedure

2.1. Material

A high-purity coarse-grained niobium ingot was obtained by means of multiple electron-beam melting. Interstitial (O < 50, N < 5, wt. ppm) and metallic (W < 55, Fe < 45, Al < 30 and Si < 50, wt. ppm) impurity contents are in agreement with ASTM-B-391-99 (reactor grade). In the initial state the ingot consisted of columnar grains with grain boundaries lying nearly parallel to the longitudinal direction. These grains are 10–30-mm wide and 40–200-mm long in average. Larger grains are often found. A 10-mm-thick bicrystal was cut out from the center of this ingot and then rolled at room temperature without intermediary annealing to a total reduction in thickness of 70% in multiple passes. Three nominal reductions were chosen to characterize its microstructural evolution upon cold rolling, i.e. 33, 50, and 70%. The prior grain boundary (referred to the as-cast condition) was positioned nearly parallel to the rolling direction (RD). The microstructure of this bicrystal, formed by grains A and B, was investigated in the cold-worked state and after vacuum annealing at 800 and 900 °C for 1 h. The investigation of the microstructure was focussed in banded regions found in the vicinity of the initial grain boundary to avoid surface effects on banding as those observed at the edges of the plate. Metallographic preparation of sections was carried out using conventional techniques including chemical polishing to remove surface deformation. Vickers hardness tests were carried out in deformed and annealed specimens using a Buehler Micromet 2004 microindenter with a load of 100 g (15 measurements per sample).

2.2. Microstructural characterization

The microstructure was observed in a light optical microscope under polarized light. Because of the large dimensions of this bicrystal, only selected parts of the microstructure were observed in the SEM. Channeling contrast images of selected regions were obtained in a LEO 1450-VP SEM operating at 30 kV. The EBSD scans were carried out in the rolling plane with mapped areas varying according to the magnification. Microtexture evaluation was determined by means of automatic indexing of Kikuchi patterns after suitable image processing in a TSL 2.6 system interfaced to a JEOL JSM 5800-LV SEM operating at 28 kV with a W-filament. Despite of the large applied strain (70%), the majority of the acquired Kikuchi patterns could be resolved by the software. Pole figures and misorientation distributions are based on at least 3000 single measurements for each mapped region. EBSD sampling points were performed in every 2.5–8 μm (corresponding to the map pixel size). Misorientation profiles were also determined in linescans across deformation bands.

3. Results

3.1. Microstructure in the cold-worked state

The initial orientation of grains A and B was close to (221)[434] and (102)[101], respectively (for details, see [5]). The behavior of these two grains concerning work hardening is shown in Fig. 1. Hardness was determined in both grains after every rolling pass. Hardness tests were performed along a straight line from the grain boundary towards the edge of the specimen. Standard deviation of hardness tests increases with strain indicating that the amount of work hardening varies from the grain boundary to the edge. Grain B work-hardened more than grain A in the investigated range of plastic

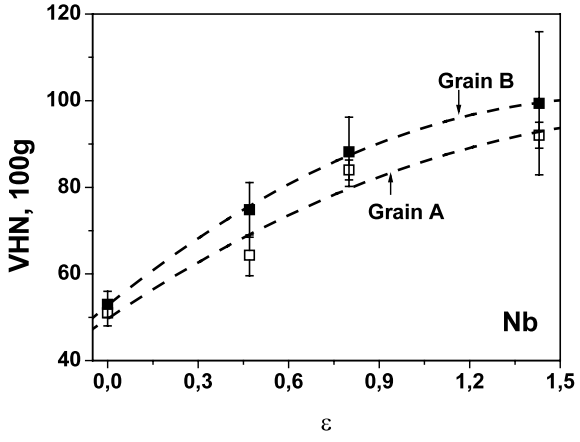

Fig. 1. Work-hardening behavior of grains A and B during cold rolling.

strain. This difference in hardness, which reflects the amount of stored energy, influenced the recrystallization kinetics in both grains (see Section 3.3).

Fig. 2 shows an overview of the longitudinal section of grain B after rolling using light optical microscopy. Banding was more pronounced in this grain. It is important to note that the micrographs shown in Fig. 2 are not consecutive, i.e. after every chosen reduction grain B was not sampled following one after the other. This procedure explains the changes in morphology and direction taken by bands from one micrograph to another. Banding is evident in all micrographs. Details of these bands can be better resolved at SEM in the backscattered mode. Fig. 3a shows a colony of bands in grain B after 33% reduction. The orientation contrast provided by backscattered electrons allows to distinguish regions of extension above about 1 μm with misorientations relative to their neighborhood by more than 1° (this does not exclude presence of misorientations above 1° provided that the crystallite size is less than 1 μm). A sharp contrast is observed in the immediate vicinity of the band–matrix interface. These structures can be resolved in detail only by using TEM, however, SEM enables the visualization of these narrow bands, about 2 μm wide (see arrows). Fig. 3b displays a

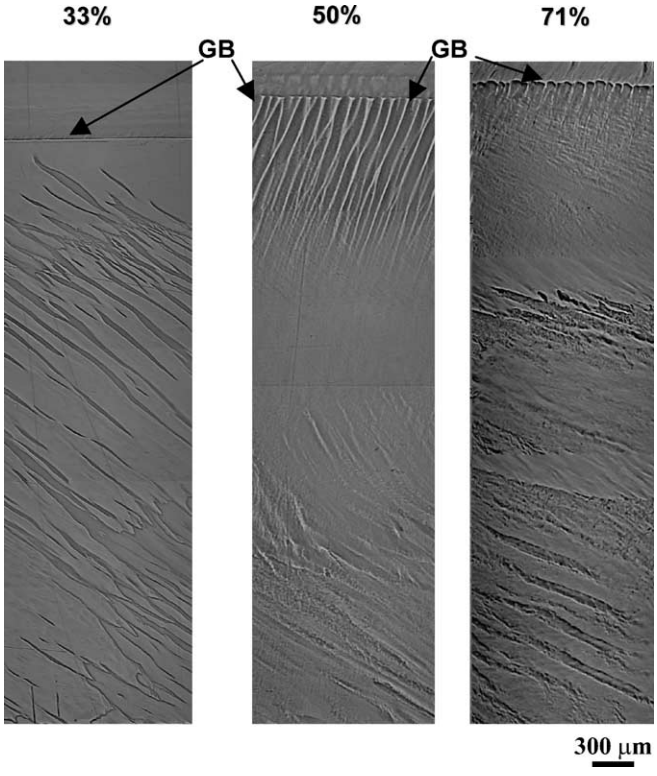

Fig. 2. Band morphology revealed by longitudinal sections of grain B deformed to: (a) 33%, (b) 50%, and (c) 70%. LOM. Samples were taken in distinct regions of grain B for illustrative purposes. These micrographs are not consecutive.

a)

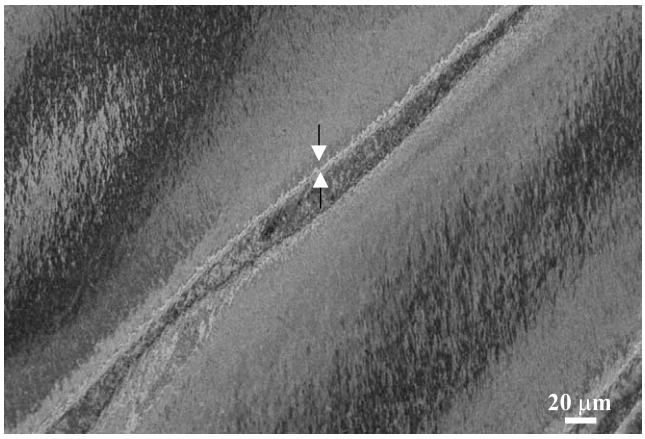

b)

Fig. 3. Channeling contrast micrographs of longitudinal sections of grain B 33% rolled showing macro-scale bands. Contrast provided by this technique enables the visualization of details of the substructure.

deformation band, about 20 μm wide, in the interior of the same grain. This band is bounded, on both sides, by narrower structures (brighter contrast) resembling transition bands.

Warped bands are predominant in the microstructure of both grains and are commonly arranged in colonies. These colonies intersect each other in many parts of the microstructure. The width of bands also varies. In average, bands were found having 20–100 μm in width, tending to become narrower and more closely spaced with increasing strain.

The differences in terms of band morphology can be visualized in the transverse section of both grains. For sake of simplicity, Fig. 4 shows the transverse section of both grains deformed up to 70%. It is evident that the whole microstructure is banded in both grains, however, plate-like bands are predominat whereas the morphology of bands in grain B is somewhat more complex. These coarse bands make angles of about 5° with the RD in grain A. Families of finer bands are arranged in

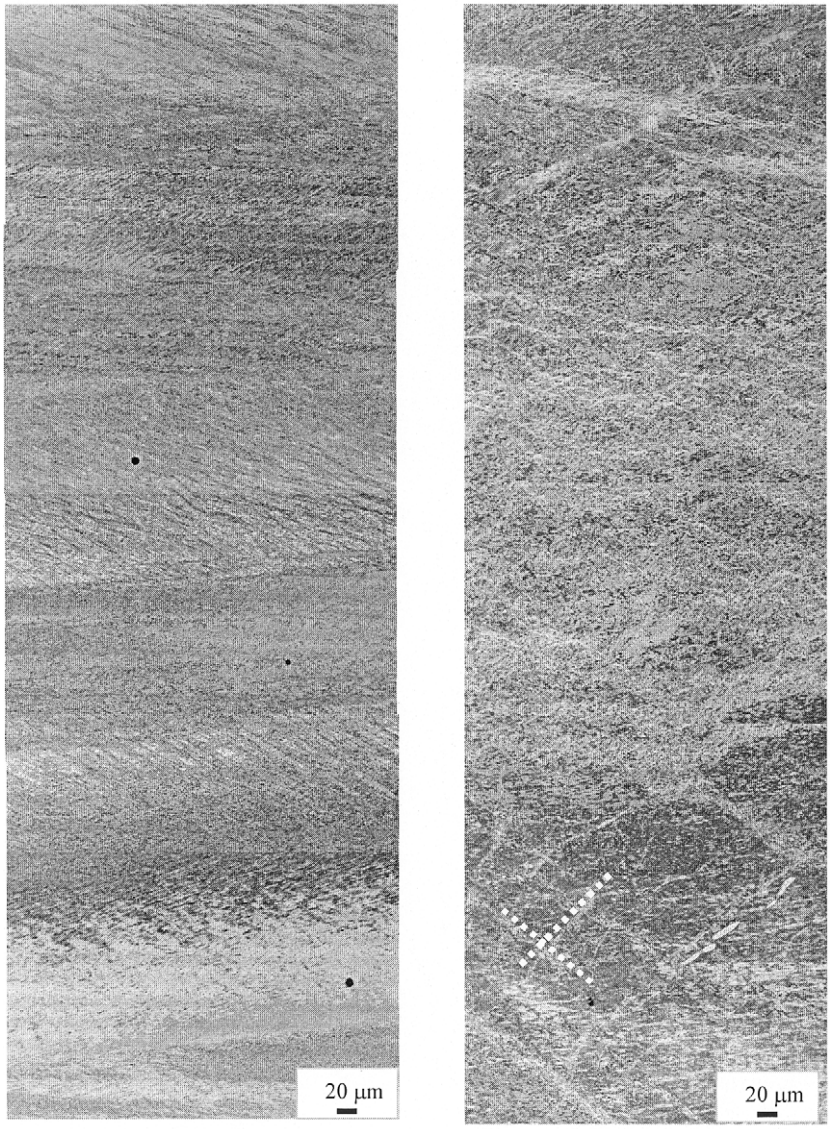

Fig. 4. Channeling contrast micrographs of the transversal section of grains (a) A, and (b) B after 70% reduction. The height of these micrographs correspond to the thickness of each grain.

parallel within each coarse band in this grain. They also alter in orientation from one part to another along its thickness. In grain B distinct colonies of bands intersect each other from one side to another at angles close to 70° (see dashed lines in the lower part of Fig. 4b).

3.2. Misorientations across bands in the cold-worked state

EBSD orientation maps show that large lattice rotations occur within these coarse grains during cold rolling. The misorientations (ψ) across banded regions were determined using random linescans. Figs. 5 and 6 show, respectively, the results of EBSD measurements in selected regions of grains A and B. Both grains were sampled after reductions of 33, 50 and 70%.

Grain A showed regions subdivided by low-misoriented boundaries, below 5° in average for 33 and 50% reductions. These profiles show the presence of one intense peak corresponding to a banded region. The remaining peaks have misorientations lower than 2° reflecting the nature of the substructure developed in the vicinity of these bands. In the most deformed specimen (Fig. 5c), a banded structure was mapped revealing the occurrence of many boundaries with high-angle character. DB along RD is associated with strong RD and transverse direction (TD) rotations. Values of ψ of about 55° are commonly observed. These bands are similar to those shown in Fig. 3a. Due to intrinsic

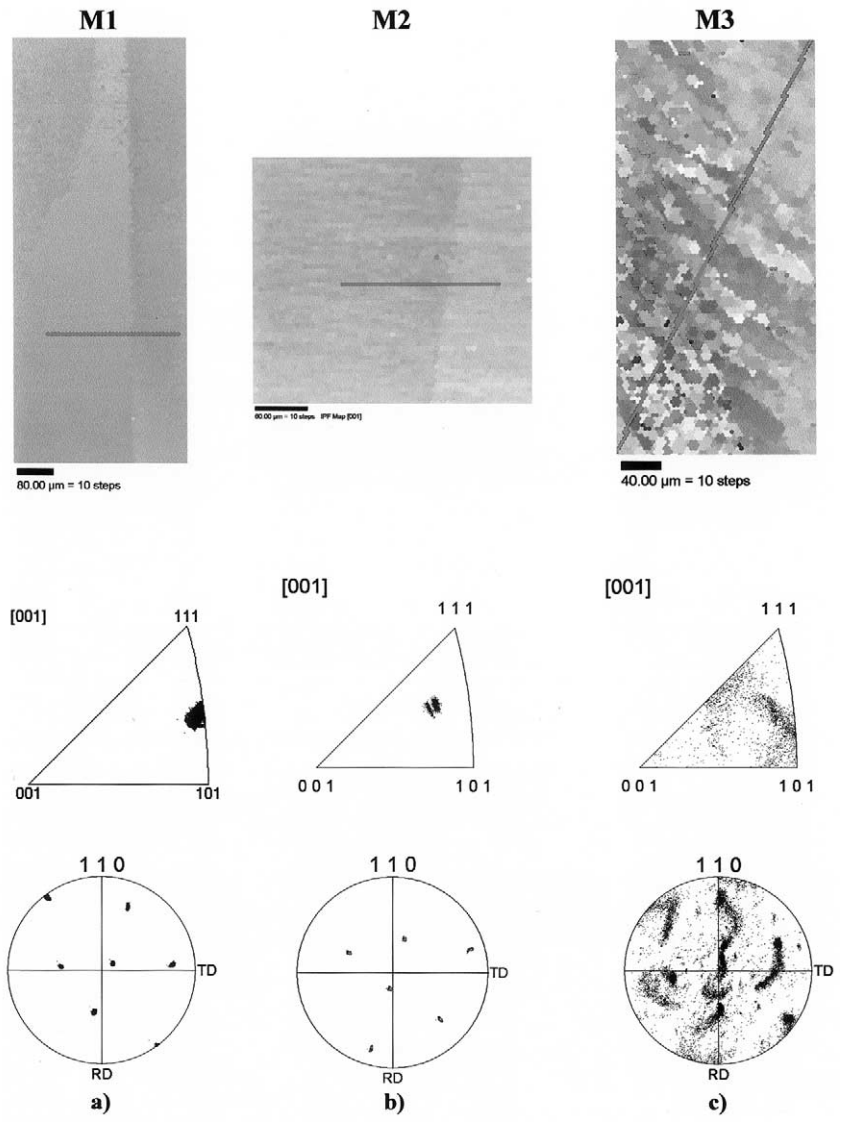

Fig. 5. Orientation mapping, pole figures at (110) and inverse pole figures at RD in distinct banded regions of grain A deformed to: (a) 33%; (b) 50%, and (c) 70%. RD is perpendicular to the scale bar.

limitations of the EBSD technique, transition bands cannot be resolved in detail, even using a smaller pixel size and higher magnifications.

Contrasting with this behavior, grain B showed banded regions with predominance of high-angle boundaries even at lower reductions, as shown in Fig. 6. Regularly spaced bands are seen in Fig. 6a and b. The pole figure shown in Fig. 6b reveals the occurrence of large TD rotations during banding. Fig. 6c, on the other hand, depicts a 'calm' region in the most deformed specimen. The misorientation varies a few degrees ($\psi < 8^\circ$) within this region whereas very high values, up to 55°, are found when the linescan intersect a colony of bands (see lower part of Fig. 6c).

The orientation spread across these boundaries can be easily visualized when the values of ψ are plotted against distance in a single linescan. Fig. 7 shows the misorientation profiles corresponding to the mapped areas named M1–M6 shown in Fig. 5 and Fig. 6. These profiles reveal the existence of an alternating pattern in terms of misorientations. 'Calm' areas corresponding to the matrix regions (also subdivided, but in a lesser extent) are interspersed with strongly rotated bands. Banding interspacing observed in the microstructure and also in the orientation maps is equivalent to the periodicity observed in the misorientation profiles.

3.3. Recrystallization

Table 1 shows the softening behavior of grains A and B during vacuum annealing. Note that the most pronounced softening occurs at 900 °C due to recrys-

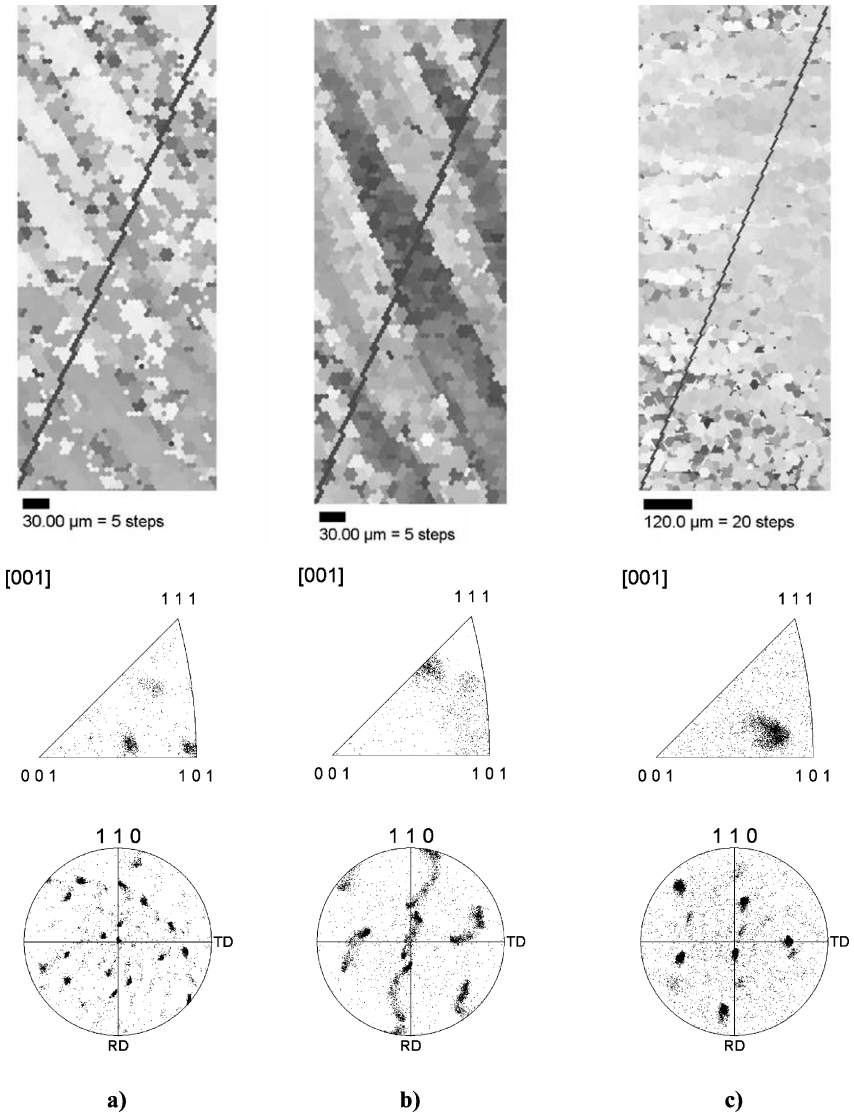

Fig. 6. Orientation mapping, pole figures at (110) and inverse pole figures at RD in distinct banded regions of grain B deformed to: (a) 33%; (b) 50%, and (c) 70%. RD is perpendicular to the scale bar.

tallization. The specimens annealed at 800 °C for 1 h displayed only partial recrystallization, with recrystallized volume fraction increasing with applied strain in both grains. Fig. 8 shows an overview of grains A and B in the annealed state. For the 33% rolled specimen, recrystallization in grain A occurred only at grain boundary region. There are no signs of recrystallization in grain A in regions far from the prior grain boundary. At the lower part of this figure, a few recrystallized grains are visible in grain B at the prior grain boundary and in banded regions.

The recrystallized fraction in grain B was also higher for 50 and 70% rolled specimens. Indeed, only a few recrystallized grains can be found in grain A after annealing at 800 °C for 1 h. For the most deformed specimen, recrystallization occurred predominantly associated to banded regions in grain A, as shown in detail in Fig. 9.

At SEM in the backscattered mode, details of the substructure of recovered regions become visible. Fig. 10 displays the so-called mosaic structure surrounded by new grains in the specimen 33% rolled and annealed at 900 °C for 1 h. The substructure consists of nearly elongated subgrains with sizes close to 5 μm. Note the serrated morphology of the moving grain boundaries growing towards the recovered microstructure.

Fig. 11 shows the orientation image mappings (OIM) of recrystallized grains after annealing at 800 °C for 1 h. Fig. 11a shows grains nucleated at the grain boundary of former grains A and B. These cube- and close-to-cube-oriented grains are found along the whole grain boundary, however, they exerted a minor influence on

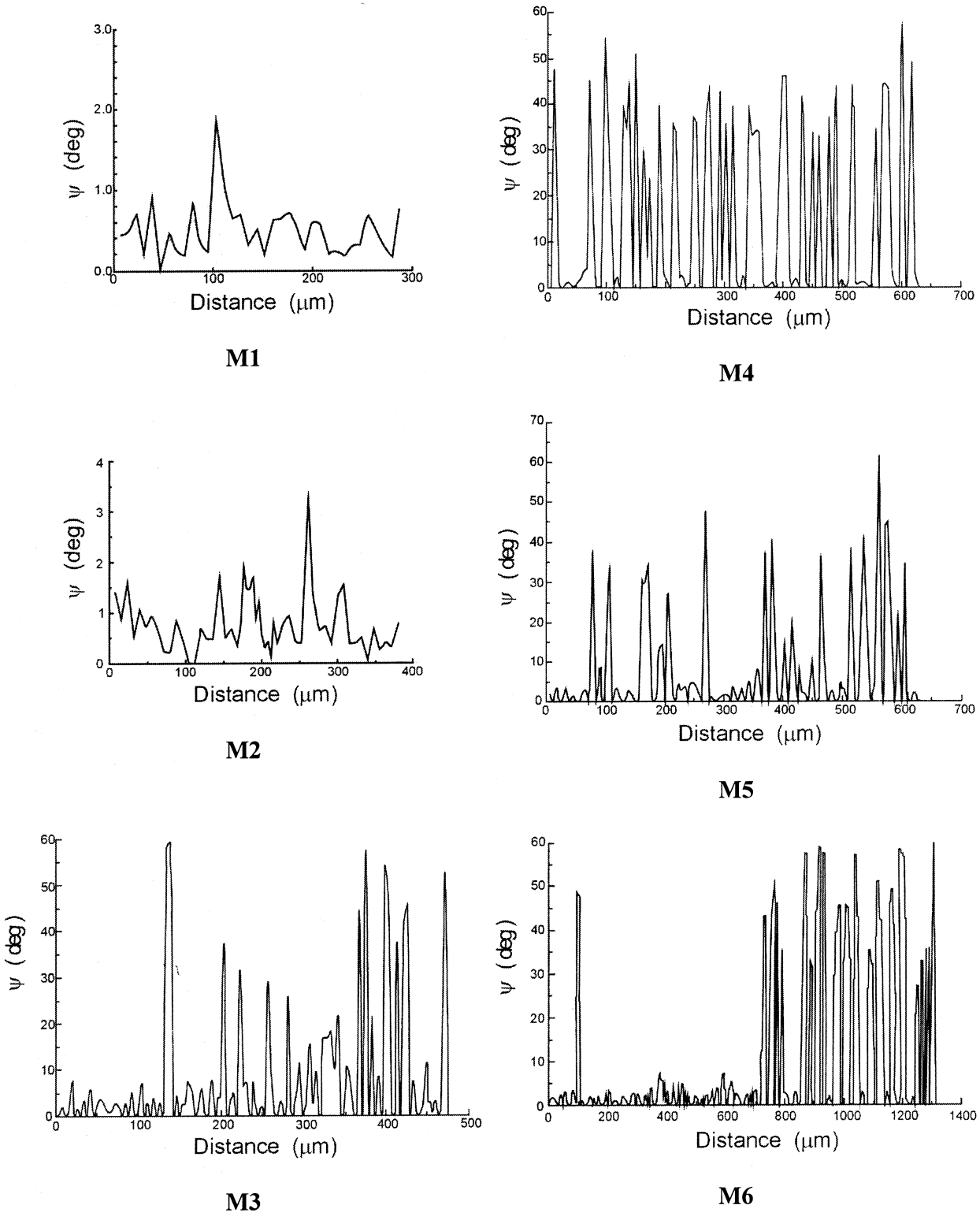

Fig. 7. Misorientation profiles corresponding to the mapped areas shown in Figs. 5 and 6.

the final recrystallization texture of both grains. Fig. 11b and c show recrystallized grains nucleated at a deformation band lying parallel to the RD. Independently of the applied strain, these cube- and close-to-cube-oriented grains were predominant at the beginning of the recrystallization of this bicrystal.

Recrystallization was almost complete in both grains after 70% reduction as shown in Fig. 12. From this

Table 1
Softening behavior of grains A and B during vacuum annealing at 800 and 900 °C for 1 h

Reduction (%)	Deformed state		800 °C for 1 h		900 °C for 1 h	
	Grain A	Grain B	Grain A	Grain B	Grain A	Grain B
0	51±3	53±3	–	–	–	–
33	64±5	75±6	62±4	70±9	61±3	55±5
50	84±2	88±8	78±3	75±6	57±9	53±2
70	92±3	100±16	64±11	85±9	52±3	50±2

Hardness is expressed as VHN.

figure, it is evident that grain size and grain morphology vary markedly from region to region. Grain size in former grain A is in the mm-range. Grain B, on the other hand, gives rise to a finer structure with sizes close to 400 μm. A close inspection at the experimental ODFs obtained from EBSD data shown in Fig. 12 reveals the existence of a diffuse recrystallization texture around $\{051\}\langle 4\bar{1}3\rangle$ in former grain B. The interpretation of the

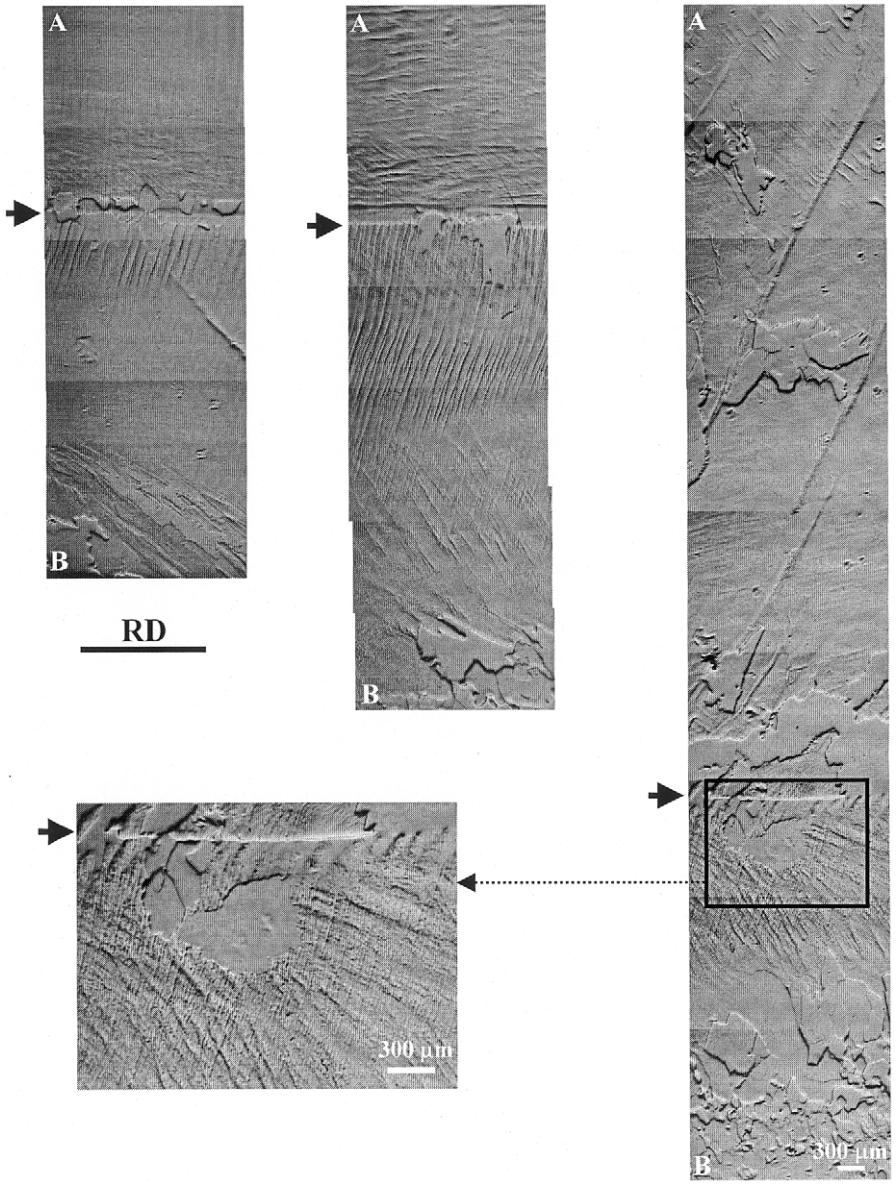

Fig. 8. General view of the microstructure of grains A and B after annealing at 800 °C for 1 h (LOM). Marker refers to all micrographs. Arrows mark the position of the original grain boundary. RD is also common to all micrographs.

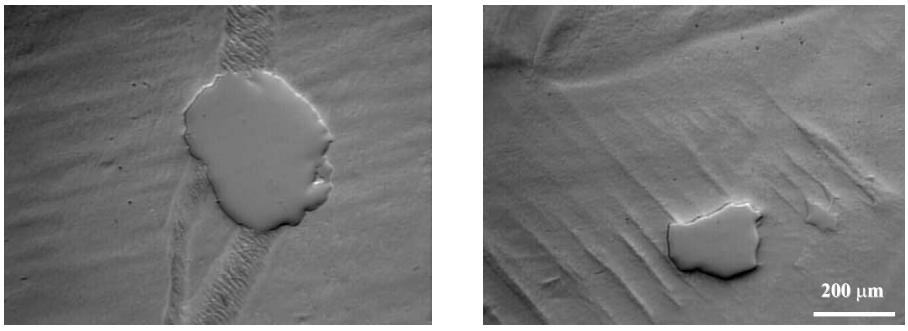

Fig. 9. Details of favored nucleation at deformation bands in grain A 70% rolled after annealing at 800 °C for 1 h (LOM). Marker is common to both micrographs.

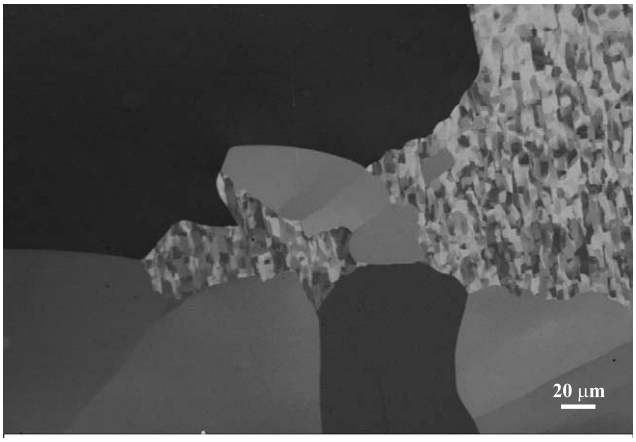

Fig. 10. Channeling constrast micrograph revealing details of the recovered microstructure in a partially recrystallized specimen 33% deformed and annealed at 900 °C for 1 h. Recrystallized grains surrounding the substructure are easily seen.

recrystallization texture found in grain A is more complicated. The major component is nearly centered in $\{021\}\langle 501\rangle$. A weaker $\{013\}\langle 9\bar{4}1\rangle$ component also appears.

4. Discussion

The plastic deformation of coarse-grained materials usually leads to a very inhomogeneous microstructure [2,6,7]. The homogeneous deformation of grains assumed in the Taylor model is not valid when grains fragment in many parts [7]. Deformation bands are commonly reported and provide highly misoriented boundaries within these coarse grains acting as favorable sites for recrystallization upon further annealing [8,9]. The high amount of stored energy in a structure containing bands is explained by the high density of geometrically necessary dislocations forming such boundaries. Upon further annealing, the potential nuclei gain the necessary mobility to grow driven by the remaining energy stored in the recovered structure. The preferential nucleation of new grains at sharp boundaries and growth upon subsequent annealing has been reported in aluminium [10], copper and copper alloys [11,12], iron [13] and interstitial-free steels [14], just to bring a few examples.

DB is grain-size dependent [1,7]. The deformation structure tends to be more homogeneous in fine-grained materials than in coarse-grained ones. An extensive discussion about this subject was presented by Hansen [7]. The results shown in this paper confirm that DB is an effective mechanism of grain fragmentation in coarse-grained niobium. With increasing strain, new dislocation structures evolve and new high-angle boundaries arise subdividing the microstructure. In consequence of the large stored energy and lattice curvatures associated to these boundaries, DB plays an important role in recrystallization of coarse-grained materials. At this point, it is opportune to emphasize that the total area of boundaries provided by deformation bands is much larger than the whole grain boundary area available in coarse-grained materials [15]. Vandermeer and Juul Jensen [16] have demonstrated the importance of two-dimensional surfaces on preferred grain nucleation during recrystallization of copper. The planar array of dislocations in deformation bands is a good example of such two-dimensional surfaces. In addition to the grains nucleated at deformation heterogeneities, new grains were also observed at the prior grain boundary, as expected. Hirth [17] showed that dislocations substructures with higher misorientations develop in the vicinity of grain boundaries due to the intensive dislocation interaction. For this reason, the first recrystallized grains are expected to be found predominantly at these preferential sites. As a general comment, the presence of deformation heterogeneities or regions of localized deformation in the interior of the grains and orientation perturbations [18,19] found in the vicinity of grain boundaries (from the as-cast structure) appear to govern the early stages of recrystallization in coarse grained niobium.

DB is also orientation dependent. This has been established for fcc metals (in Cu and Al, for instance) [11]. In the case of bcc metals, DB in compression was

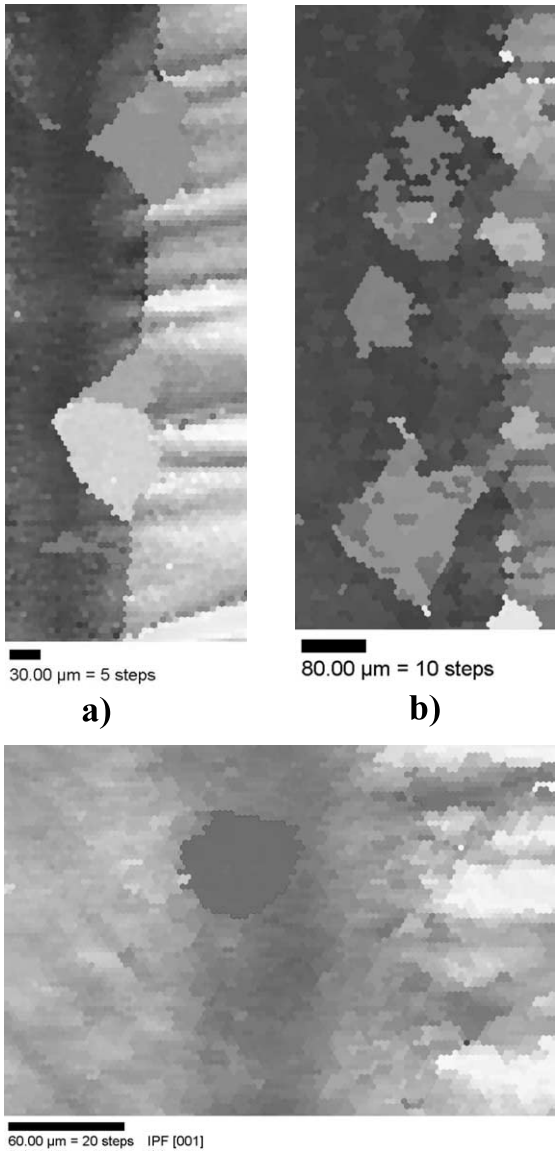

Fig. 11. OIM of the bicrystal annealed at 800 °C for 1 h: (a) grain boundary region of the 33% rolled bicrystal; (b) 33% rolled bicrystal showing cube- and close-to-cube-oriented grains nucleated at the deformation band; (c) 50% rolled bicrystal showing one cube-oriented grain nucleated at the deformation band. In all micrographs, grain A is positioned at the left side. RD is parallel to the vertical axis.

associated with the unstable orientations belonging to ⟨110⟩ [13]. Dillamore et al. [20] have shown that orientations for which the compression axis lay between ⟨110⟩ and ⟨411⟩ are more likely to form DBs. These results were observed in specimens deformed by uniaxial compression. Although the deformation mode employed in the present work is cold rolling, a similar behavior is found. Grain A showed a less pronounced banding compared with grain B, as shown in Fig. 2. The ⟨110⟩-orientation component associated to the matrix (less rotated regions of the crystal) is present at the banded regions mapped in grain B, as clearly shown in Fig. 6a and c.

The misorientations across DBs varied from region to region within individual grains and also from one grain to another. These rotations may vary locally because of the crystallographic constraints imposed by the prior grain boundary and also by geometric and friction effects during rolling. These aspects contribute to the occurrence of bands with distinct morphology and spacing from region to region. Based on the results of EBSD mappings along these large grains, a non-uniform spatial distribution of textures in the deformed state is evident.

The lattice curvatures associated to the DBs observed in the present work are similar to those found in the literature. Inokuti and Doherty [13] reported misorientations developed during compression tests in pure iron as high as 50° in 40% compressed samples. Aluminum single crystals deformed in compression have also shown misorientations of 25° in average following a strain of 0.45 [9]. These two examples corroborate the magnitude of misorientation angles across the high angle boundaries shown in the current work. The knowledge of the magnitude of the misorientation angles formed during grain fragmentation is essential to the development of further models to predict recrystallization behavior in coarse-grained niobium.

The early stages of recrystallization can be investigated in detail when annealing is performed at moderate temperatures, e.g. 800 °C (see Figs. 8 and 11). The first grains grow enough to be visualized easing the identification of preferential nucleation sites. If recrystallization annealing is performed at very high temperatures, this information cannot be drawn in a straight manner from metallographic observations.

The microstructure of recovered regions in partially recrystallized specimens also deserves a special attention. To our knowledge, the mosaic-like structure shown in the present work (see Fig. 10), which is well known from Al-alloys [21,22], has not yet been reported in niobium, at least using channeling constrast. A similar feature has been also reported in coarse-grained tantalum deformed by cold swaging [23]. The misorientations present in the mosaic structure are not necessarily large. Rather it is supposed that the mosaic boundaries are nonpermanent subgrain boundaries which do not turn into the longitudinal direction like lamellar boundaries and enclose large enough regions of similar orientation to show up in SEM.

The inhomogeneity in terms of the recrystallization microtexture observed in oligocrystalline niobium has been reported in an earlier paper [24]. This inhomogeneity is predominantly related to orientation effects. Concerning the results presented in this paper, the difference in terms of grain size in the recrystallized state has probably to do with nucleation. Because of the

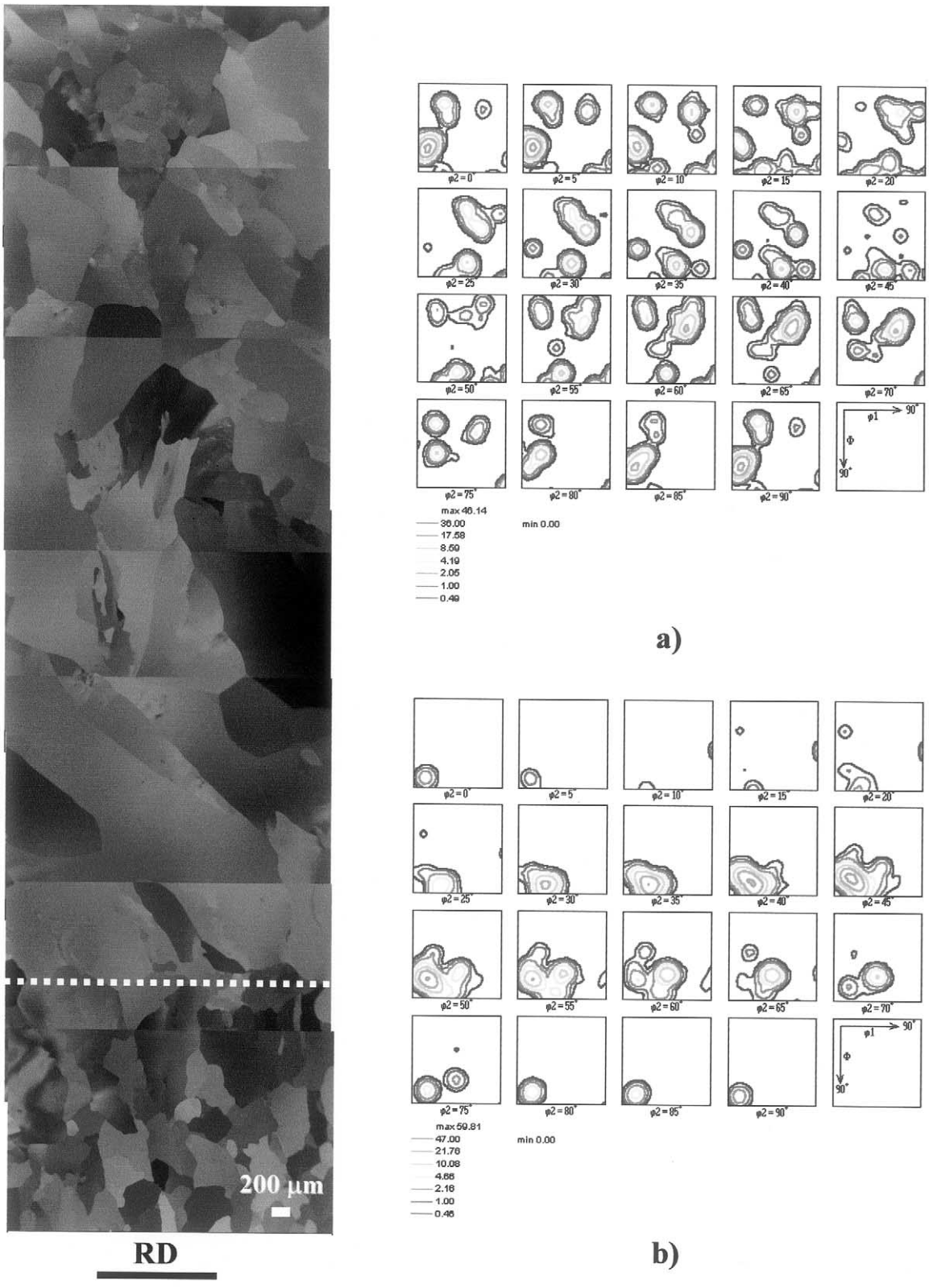

Fig. 12. General view of the microstructure of the 70% rolled bicrystal after annealing at 900 °C for 1 h: (a) experimental ODF corresponding to the mapping of the coarser grains (above dashed line); (b) experimental ODF corresponding to the finer grains (below dashed line).

higher amount of highly-misoriented bands in former grain B, nucleation occurred in a larger extent, giving rise to finer grains after annealing. The recrystallized grain size found in the Nb slab reported in [24] also

varied in a sharp manner from one texture component to another, as we have seen in the present work.

5. Conclusions

In the present work, we demonstrate the pronounced heterogeneity of the microstructure of a niobium bicrystal deformed to various strains by cold rolling. Noticeable differences in grain subdivision were observed in two adjacent grains (A and B) using channeling contrast at SEM combined with orientation mapping provided by EBSD measurements. A non-uniform spatial distribution of textures in the deformed state is evident. Grain B subdivided into deformation bands bounded by a wide range of misorientations, mostly having high angle character. Grain A, on the other hand, exhibited deformation bands with $\psi < 5^\circ$ for 33 and 50% reductions. The stored energy varied markedly one grain to another and, in consequence, the recrystallization behavior. Recrystallization in this coarse-grained niobium bicrystal started preferentially at the banded regions and in the vicinity of the prior grain boundary, independently of the applied strain. Distinct recrystallization textures were found in both grains after annealing at 900 °C for 1 h.

Acknowledgements

Sincere thanks are due to Fundação de Amparo à Pesquisa do Estado de São Paulo (FAPESP) for the financial support of this work (Grant no. 99/11756-0). J.F.C. Lins is also grateful to FAPESP for his scholarship (Grant no. 00/00706-0). Thanks are due to Dr Paulo Rangel Rios (UFF, Brazil) and to Dr Ronald Lesley Plaut (USP, Brazil) for going through the manuscript meticulously. One of us (H.R.Z. Sandim) is CNPq fellow under Contract No. 300158/02-5.

References

[1] C.S. Lee, B.J. Duggan, R.E. Smallman, Acta Metall. Mater. 41 (1993) 2265.
[2] D.A. Hughes, in: E.N.C. Dalder, T. Grobstein, C.S. Olsen (Eds.), Evolution of Refractory Metals and Alloys, The Minerals, Metals & Materials Society, Warrendale, 1994, p. 219.
[3] D.J. Dingley, V. Randle, J. Mater. Sci. 27 (1992) 4545.
[4] F.J. Humphreys, J. Microsc. 195 (1999) 170.
[5] J.F.C. Lins, Dissertation, FAENQUIL, Lorena, 2002.
[6] N. Hansen, Mater. Sci. Technol. 6 (1990) 1039.
[7] N. Hansen, Metall. Trans. 16A (1985) 2167.
[8] D. Kuhlmann-Wilsdorf, Acta Mater. 47 (1999) 1697.
[9] D.A. Hughes, Proceedings of the 21st Risø International Symposium on Materials Science: Recrystallization—Fundamental Aspects and Relations to Deformation Structure, Roskilde, Danmark, September 4–8, 2000, Risø National Laboratory, Roskilde, 2000, p. 49.
[10] J. Hjelen, R. Ørsund, E. Nes, Acta Metall. Mater. 39 (1991) 1377.
[11] C.S. Lee, B.J. Duggan, Acta Metall. Mater. 41 (1993) 2691.
[12] J. Hirsch, K. Lücke, M. Hatherly, Acta Metall. 36 (1988) 2905.
[13] Y. Inokuti, R.D. Doherty, Acta Metall. 26 (1978) 61.
[14] Y.Y. Tse, G.L. Liu, B.J. Duggan, Scr. Mater. 42 (2000) 25.
[15] D. Kuhlmann-Wilsdorf, S.S. Kulkarni, J.T. Moore, E.A. Starke, Jr, Metall. Trans. 30A (1999) 2491.
[16] R.A. Vandermeer, D. Juul Jensen, Metall. Trans. 26A (1995) 2227.
[17] J.P. Hirth, Metall. Trans. 3 (1972) 3047.
[18] V. Randle, N. Hansen, D. Juul Jensen, Philos. Mag. A73 (1996) 265.
[19] Q. Liu, N. Hansen, Mater. Sci. Eng. A234 (1997) 672.
[20] I.L. Dillamore, H. Katoh, K. Haslam, Textures 1 (1974) 151.
[21] M.C. Theyssier, B. Chenal, J.H. Driver, N. Hansen, Phys. Stat. Sol. (a) 149 (1995) 367.
[22] Y. Huang, F.J. Humphreys, Acta Mater. 48 (2000) 2017.
[23] H.R.Z. Sandim, H.J. McQueen, W. Blum, Scr. Mater. 42 (2000) 151.
[24] H.R.Z. Sandim, J.F.C. Lins, A.L. Pinto, A.F. Padilha, Mater. Sci. Forum. 408-4 (2002) 517.